CrossMark

ORIGINAL PAPER

Effect of reduced graphene oxide–silica composite in polyaniline: electrode material for high-performance supercapacitor

Umashankar Male[1] · Susmitha Uppugalla[1] · Palaniappan Srinivasan[1]

Abstract In order to improve the pseudocapacitance properties and cycle stability of polyaniline (PANI), reduced graphene oxide–silica (rGOS) is used to modify the polyaniline material. Ternary composites of reduced graphene oxide–silica–polyaniline (rGOSP) are prepared by chemical polymerization of aniline using ammonium persulfate oxidant with various amounts of rGOS in aq. 1 M H_2SO_4 solution. Morphology analysis of rGOSP composite revealed that the nano fibers form of polyaniline is intercalated in the graphene layers and also covered the rGOS. Symmetric supercapacitor cell is fabricated in CR2032 coin cell with rGOSP composite as electrode and its electrochemical performance is evaluated from cyclic voltammetry, galvanostatic charge–discharge, and electrochemical impedance spectroscopy techniques. rGOSP composite yielded a higher capacitance and lower ESR value compared to that of its individual components, PANI and rGOS. The energy density of the composite is found to be 10 W h kg^{-1} at a power density of 2310 W kg^{-1}. Furthermore, over 75.2 % of the original capacitance is retained after 6000 galvanostatic charge–discharge cycles at 0.8 A g^{-1}.

Keywords Ternary composite · Reduced graphene–oxide–silica–polyaniline · Supercapacitor · Button cell · Intercalation of polyaniline

✉ Palaniappan Srinivasan
palani74@rediffmail.com; palaniappan@iict.res.in

[1] Polymers & Functional Materials Division, CSIR—Indian Institute of Chemical Technology, Tarnaka, Hyderabad 500007, Telangana, India

Introduction

Research and development on conducting polymer-based materials have received a great deal of interest in the recent years because of their promising applications. Supercapacitors are charge-storage devices that have attracted great research interest, owing to their exceptional properties such as high power density, excellent reversibility, environmental protection, low maintenance cost, and long cycle life. Supercapacitors or electrochemical capacitors are classified into two major categories, electric double-layer capacitors (EDLC) based on carbon materials and pseudocapacitors (PC) based on conducting polymers and metal oxides. EDLCs store energy only at the interface, so limited capacitance is achieved, whereas in case of pseudocapacitors, high capacitance is achieved because of redox reactions involving the bulk of the material. In EDLCs, although a variety of carbon materials is being used as electrode materials in supercapacitors, graphene has attracted much research attention due to its extraordinarily high electrical and thermal conductivities, great mechanical strength, large specific surface area, low manufacturing cost, promising potential application, etc. [1–3].

Among the conducting polymers, polyaniline (PANI) is regarded as one of the most promising electrode materials due to its high electrochemical activity, low cost, environmental stability, and ease of syntheses. The capacitance of electrochemical supercapacitor arises mainly from the Faradaic reactions at the interface of electrode material and electrolyte; the charges are stored at the surface or in the bulk near the surface of the solid electrode material. Hence, the contact of the electrode material with the electrolyte plays an important role for the device to display improved capacitance. Incorporation of silica into graphene

🖄 Springer

will increase the hydrophilicity of the reduced graphene oxide–silica composite and facilitate the contact of electrode material with the electrolyte, thus, representing an opportunity for the design of materials with improved performance [4], besides increasing the surface area of the materials [5, 6]. So, the incorporation of silica modified reduced graphene oxide in polyaniline is expected to offer better properties viz., mechanical strength, permeability, thermal stability [7], and supercapacitor performance [5, 8].

Polyaniline composites with reduced graphene oxide or silica have been used as electrode materials in supercapacitor application. But, ternary composite of polyaniline, reduced graphene oxide, and silica is limited and as far as our knowledge is concerned, one report is available. Very recently, Feng et al. have reported the synthesis of polyaniline/MCM-41/graphene via in situ polymerization of aniline with MCM-41 to polyaniline–MCM-41 composite. Synthesized PANI–MCM-41 was mixed with various amounts of graphite oxide and then converted to PANI–MCM-41-G by hydrothermal procedure. The supercapacitor performance was measured in basic medium using a three-electrode system [9].

Herein, we present the synthesis and characterization of reduced graphene oxide–silica–polyaniline (rGOSP) composites. This method consists of the generation of reduced graphene oxide–silica (rGOS) by condensation of tetraethoxyortho silicate (TEOS) in the basic medium in the presence of rGO and subsequent synthesis of rGOSP composites by polymerizing aniline with rGOS. rGOSP composite is used as electrodes in button cell supercapacitors with aqueous sulfuric acid electrolyte and evaluated its performance.

Experimental

Materials and instrumentation

Aniline (S. D. Fine Chemicals, India) was distilled under reduced pressure. Graphite and TEOS (Aldrich, USA), ammonium persulfate (APS), sulfuric acid (H_2SO_4), and ammonia solution [Rankem, India] were used as received. All the reactions were carried out with distilled water, and solvents were distilled and used.

Polymer samples for Fourier transform infrared (FTIR) analysis were mixed with KBr powder and compressed into pellets, wherein the sample powder was evenly dispersed in KBr. FTIR spectra were recorded in a gas chromatography–FTIR spectrometer (model 670, Nicolet Nexus, Minnesota). X-ray diffraction (XRD) profiles for the rGOSP composite powders were obtained on a Bruker AXS D8 advance X-ray diffractometer (Karlsruhe, Germany) with CuK_α radiation ($\lambda=1.54$ Å) at a scan speed of $0.045°$ min^{-1}. The d-spacing

was calculated from the angular position 2θ of the observed reflection peaks based on the Braggs formula ($2d\sin\theta=n\lambda$), where λ is the wavelength of the X-ray beam and θ is the diffraction angle. Morphology studies of the polymer powder samples were carried out with a Hitachi S-4300 SE/N field emission scanning electron microscope (FESEM) (Hitachi, Tokyo, Japan). The polymer powder sample was sputtered on a carbon disk with the help of double-sided adhesive tape. Transmission electron microscopy (TEM) measurement was carried out with Hitachi S-5500 instrument operated at an accelerate voltage of 30 kV. The sample was prepared by casting sample dispersion on carbon-coated copper grids (300 mesh) and allowed to dry at room temperature. Thermogravimetric analysis (TGA) was performed with a TGA Q500 Universal (TA Instruments, UK) at a heating rate of 10 °C min^{-1} under nitrogen atmosphere.

Preparation of electrode and electrochemical characterization

The working electrodes were prepared by pressing the polymer sample (~2.5 mg cm^{-2}) on stainless steel mesh (316 grade) by the application of 120 kg cm^{-2} of pressure without any additional binder. The electrochemical performances of all the polymer samples were investigated using two-electrode system cells without a reference electrode. Two electrodes with an identical sample were separated by cloth and assembled as a supercapacitor. Cyclic voltammetry and galvanostatic charge–discharge experiments were performed with a WMPG1000 multichannel potentiostat/galvanostat (WonATech, Gyeonggi-do, Korea). Cyclic voltammograms (CV) were recorded from 0.0 to 0.6 V at various sweep rates, and charge–discharge experiments were performed at 0.0 to 0.6 V at various current densities. For cycle life studies, electrodes were prepared by pressing the mixture of 20 wt% of graphite and 80 wt% of polymeric sample on stainless steel mesh with the application of 120 kg cm^{-2} of pressure and the symmetric supercapacitor device was fabricated in (CR2032, Hohsen Corp.) coin cell using nonwoven fabric (polypropylene) as a separator. Electrochemical impedance spectroscopy (EIS) measurements were performed with IM6ex (Zahner-Elektrik, Germany) in the frequency range of 40 kHz to 10 mHz measured AC voltage amplitude of 10 mV referring to equilibrium open-circuit potential using three-electrode cell configuration, i.e., polymer electrode as a working electrode, platinum foil as a counter electrode, and calomel electrode as a reference electrode. All electrochemical measurements were carried out at ambient temperature, and 1 M H_2SO_4 was used as the electrolyte solution. Specific capacitance (C_s) from cyclic voltammograms is calculated using the formula $C_s=(Q\times1000)(\Delta V\times m)^{-1}$, Q is the total voltammetric charge, ΔV is

voltage window, and m is the mass of the active material. Specific capacitance (C_d) from charge–discharge curves is calculated using the formula $C_d = (2 \times i \times \Delta t)\ (\Delta V \times m)^{-1}$, where i is the constant discharge current, Δt is the discharge time, ΔV is the voltage window excluding iR drop, m is the mass of the active material. The factor of 2 comes from the fact that the total capacitance measured from the test cells is the addition of two equivalent single-electrode capacitors in series. Energy density (E_d) and power density (P_d) were calculated using the formula $E_d = (0.5 C_d V^2)(3.6)^{-1}$ and $P_d = E_d (\Delta t)^{-1}$, respectively.

Synthesis of reduced graphene oxide–silica

Reduced graphene oxide (rGO) was synthesized by a two-step procedure. First graphite was converted into graphite oxide using modified Hummer's method reported by Chen et al. [10]. In the second step, the graphite oxide was chemically reduced using hydrazine to reduced graphene oxide [11]. A composite of rGO and silica was prepared by following the reported procedure [4]. rGO (1 g) was dispersed in a mixture of 100 mL distilled water and 100 mL ethanol, and the mixture was homogenized using PDH for 10 min at 10,000 rpm and 3.7 mL of TEOS was added immediately. pH of the mixture was maintained at 9–11 using ammonia solution. The mixture was kept at 60 °C under constant stirring for 24 h. This mixture was filtered, washed with distilled water, followed by acetone, and dried at 50 °C in an oven.

Synthesis of reduced graphene oxide–silica–polyaniline composite

A series of rGOSP samples was prepared by varying amounts of rGOS with a constant amount of aniline (Table 1). In a typical procedure, a particular amount of rGOS was dispersed in 50 mL of 1 M H_2SO_4 containing 0.25 g of aniline in a 100-mL beaker and sonicated until uniform dispersion then 0.57 g of APS pre-dissolved in 50 mL of 1 M H_2SO_4 solution was added. The reaction mixture was stirred for 4 h at room temperature. The resulting reaction mixture was filtered under vacuum, washed with an ample amount of distilled water and acetone. The powder sample was dried at 50 °C until a constant weight.

Results and discussion

Reduced graphene oxide–silica (rGOS) composite was prepared from the condensation of TEOS in the presence of rGO using the reported procedure [4]. To increase the electrochemical performance of conducting polymer polyaniline, rGOS was incorporated into the polyaniline (PANI) system via an aqueous polymerization pathway by oxidizing aniline using ammonium persulfate in the presence of rGOS. The reaction scheme is given in Scheme 1. The amount of rGOS was varied from 20 to 100 wt.% with respect to the amount of aniline used in the reaction. Yield of rGOSPs is reported in Table 1.

In order to select a suitable material for supercapacitor among rGOSP hybrid materials, cyclic voltammetry as well as charge–discharge analysis was performed for symmetric cell configuration and the results are compared with that of its individual components, rGOS and PANI.

CV for rGOSP symmetric cells were carried out with a higher sweep rate of 10 mV s^{-1} in 1 M H_2SO_4 electrolyte solution and are represented in Fig. 1a. It is clearly seen from the figure that the CV is almost rectangular with good symmetry, showing a good capacitive behavior of the materials. Small humps observed are due to redox processes of the electrode.
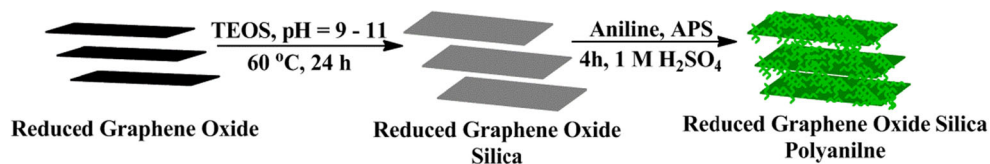
Among the rGOSP composites, rGOSP20 shows a good voltammetric current response followed by rGOSP40, rGOSP60, rGOSP80, and rGOSP100. As current response is a direct measure of the charge stored by the material, it confirms that the rGOSP20 has the highest specific capacitance (C_s), 338 F g^{-1} and the C_s value decreases to 278, 261, 199, and 164 F g^{-1} as the amount of rGOS increases in the composite. A similar trend was found in lower sweep rates also, i.e., at 1 and 5 mV s^{-1} (Fig. 1b). This is caused by the incorporation of less electrochemically active rGOS in the composite. The value of C_s observed for PANI and rGOS is found to be 205 and 52 F g^{-1}, respectively, which are lower than that of its composite, rGOSP20 (338 F g^{-1}).

FTIR spectra of PANI, rGOS, and rGOSP20 are depicted in Fig. 2. Major peaks of PANI obtained are close to those of characteristic peaks of reported polyaniline salt [12], peak at 3445 cm^{-1} (N–H str.), 3260 cm^{-1} (NH$^+$—indicative of doping, i.e., salt formation), 1560 cm^{-1} (C=C str., quinonoid ring), 1475 cm^{-1} (C=C str., benzenoid ring), 1295 cm^{-1} (C–N str., quinonoid ring), 1240 cm^{-1} (C–N str., benzenoid ring),

Table 1 Yield of reduced graphene oxide–silica–polyaniline composites with varying amounts of graphene–silica

Experiment	50 mL 1 M H_2SO_4		50 mL 1 M H_2SO_4	Yield (g)
	Aniline (mg)	rGOS (mg)	APS (g)	
rGOSP20	250	50	0.57	0.25
rGOSP40		100	Reaction time: 4 h	0.25
rGOSP60		150		0.30
rGOSP80		200		0.29
rGOSP100		250		0.32

Scheme 1 Schematic representation for the preparation of rGOSP composite

Reduced Graphene Oxide → (TEOS, pH = 9 - 11, 60 °C, 24 h) → Reduced Graphene Oxide Silica → (Aniline, APS, 4 h, 1 M H$_2$SO$_4$) → Reduced Graphene Oxide Silica Polyanilne

1105 cm^{-1} (N=Q=N vibration, where Q represents the quionoid ring), and 800 cm^{-1} (1,4-disubstituted benzene). IR spectrum of pure rGOS shows a peak at 3425 cm^{-1} corresponding to O–H group of graphene, peaks at 2875 and 2925 cm^{-1} corresponding to aromatic sp^2 C–H stretching of graphene [13], 1090 and 810 cm^{-1} corresponding to Si–O–Si asymmetric and symmetric stretching, respectively, [14]. On careful examination of IR spectrum of rGOSP20 sample, major peaks obtained at 3450, 2920, 1560, 1475, 1295, 1240, 1105, and 800 cm^{-1} are very similar to the IR spectrum of PANI and peaks due to rGOS is not visible in the spectrum. These results indicate that rGOS is covered by PANI.

XRD patterns of PANI, rGOS, and rGOSP20 are shown in Fig. 3. XRD spectrum of PANI shows two major peaks at d-spacing of 3.54 and 4.63, and rGOS shows peaks at 2.11, 3.6, and 4.48. The peaks at 2.11 and 3.6 are due to the presence of graphite-like structures from reduced graphene oxide [11, 15, 16]. Additionally, the peak at 3.6 has a broad shoulder at 4.63, presumably induced by a bimodal or multimodal character of the interlayer spacing of rGO powder [11] and the peak at 3.6 also confirms the presence of amorphous silica on rGOS [4, 17]. The XRD patterns of all the rGOSP samples are very nearly the sample. As a representative system, XRD spectrum of rGOSP20 shows peaks at 2.11, 3.54, 4.49, and 14.25. The first peak indicates the presence of rGOS, the second and third peaks indicate the presence of PANI. The last diffraction peak at a smaller angle, i.e., with a

d-spacing of 14.2, indicates the intercalation of PANI in graphene [16]. The XRD patterns verify not only the intercalation of PANI chains between rGOS sheets but also the coexistence of rGOS and PANI in the rGOSP.

FESEM images of rGO, rGOS, and rGOSP are given in Fig. 4. FESEM pictures of rGO show stacked layered morphology (Fig. 4a). FESEM of rGOS (Fig. 4b) shows little exfoliated layer morphology compared to rGO. This is due to the formation of silica and intercalation on and in between the rGO layer during the synthesis of rGOS. Polymerization of aniline with rGOS results in a nano fibrous network of PANI with diameters ranging from 15 to 20 nm and length 50 to 100 nm (Fig. 4c) and uniformly grown and covered the rGOS. The homogeneous coating of PANI onto the rGOS layers is due to the interaction of polyaniline electron donor with the surfaces of rGOS electron acceptor and also the strong π–π interaction between the backbones of PANI and the rGOS [18]. Moreover, the nano fibrous morphology of PANI may provide a large specific surface area and is of benefit to the ion diffusion and migration [19, 20]. The nano fibrous morphology of PANI in rGOSP is also confirmed through TEM image (Fig. 4d, e). EDX spectra of rGOS and rGOSP composites support the presence of silica element.

Thermograms of PANI, rGOS, and rGOSP20 are shown in Fig. 5. rGOS is stable up to 500 °C. Thermogram of rGOSP20 is more or less similar to that of the thermogram of PANI. First step weight loss up to 110 °C is due to the loss of water molecules, and the polymer is stable
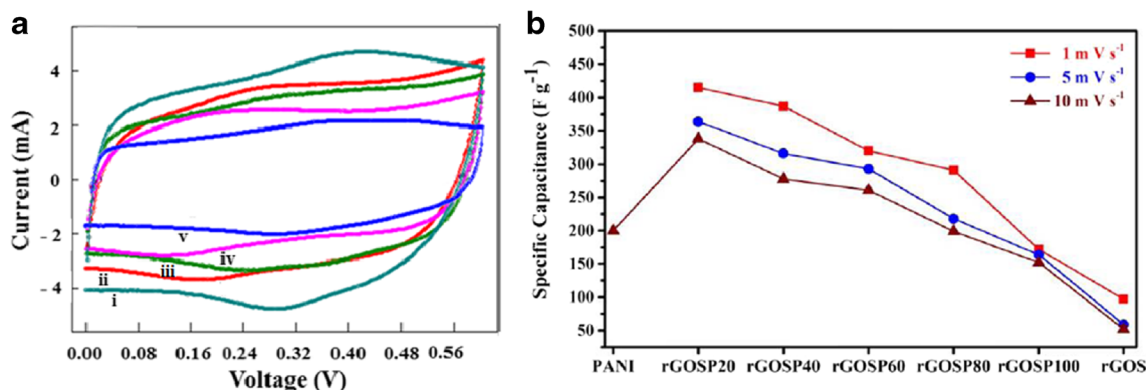
Fig. 1 **a** Cyclic voltammograms of the rGOSP composites (*i*) rGOSP20, (*ii*) rGOSP40, (*iii*) rGOSP60, (*iv*) rGOSP80, and (*v*) rGOSP100 in 1 M H$_2$SO$_4$ electrolyte measured at a sweep rate of 10 mV s^{-1} and **b** comparison of the specific capacitance of rGOS, PANI, and rGOSP composites measured at various sweep rates
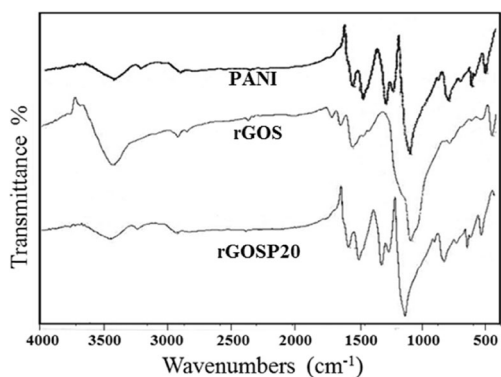
Fig. 2 FTIR spectra of PANI, rGOS, and rGOSP20

up to 250 °C. In fact, a considerable amount of water is essential for an electrode material as it is conducive for ionic transportation in an electrolyte, thus enhancing electrochemical performance [21–23]. However, weight loss at 250 °C is found to be lower in the case of rGOSP20 (14 %) compared to that of PANI (18 %). Higher thermal stability of rGOSP20 is caused by the incorporation of relatively stable rGOS (6 % weight loss at 250 °C) in rGOSP20.

Galvanostatic charge–discharge experiments are carried out for rGOSP composites in the potential range of 0 to 0.6 V at a current density of 0.4 A g^{-1} and are represented in Fig. 6a. The charge–discharge curves are with good triangular symmetry demonstrating the excellent capacitive properties of the composite materials, although a little iR drop is observed. Slight deviation from the linearity of charge–discharge curves is due to the redox process associated with electrode materials. Specific capacitance values at different current densities for PANI, rGOS, and rGOSPs are calculated and are shown in Fig. 6b. C_d values calculated at a charge–discharge current density of 0.4 A g^{-1} are found to be decreasing with increasing amount of rGOS.

Among the rGOSP composites, rGOSP20 shows a higher capacitance value (318 F g^{-1}), which in turn, higher than that of its individual components, PANI (300 F g^{-1}) and rGOS
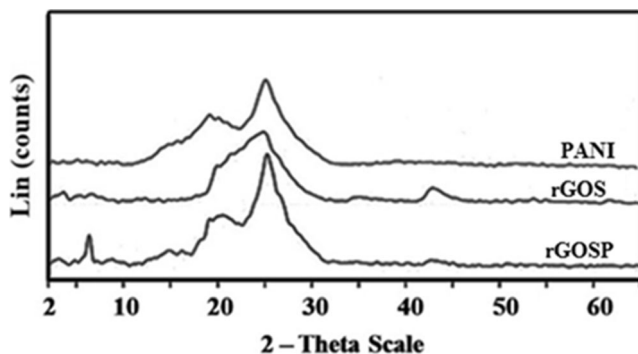

Fig. 3 XRD patterns of PANI, rGOS, and rGOSP20

(28 F g^{-1}). Even at higher charge–discharge current density of 0.8 A g^{-1}, the obtained capacitance of rGOSP20 is 305 F g^{-1}, which is much higher than that of PANI (200 F g^{-1}). The rate capability of the rGOSP20 electrode, i.e., the behavior of specific capacitance with applied current density is shown in Fig. 6c. The high specific capacitance of 205 F g^{-1} obtained even at a high current density of 4 A g^{-1} represents the good rate capability of the electrode material. C_d values are found to be 335, 318, 305, 256, and 205 F g^{-1} at current densities of 0.2, 0.4, 0.8, 2, and 4 A g^{-1}, respectively. This result indicates that the button cell can work even at higher discharge rates. The value of the energy density versus power density for rGOSP20 composite material is calculated, and the value of energy density is found to be 17, 16, 15, 13, and 10 W h kg^{-1} at power densities of 0.1, 0.2, 0.5, 1.1, and 2.3 kW kg^{-1}, respectively. Charge–discharge experiments have been carried out up to 0.6 V because in aqueous solutions, polyaniline tends to degrade at higher potentials more than 0.6 V [24].

In order to find out the cycling stability, charge–discharge experiments are carried on rGOSP20 and PANI systems at a current density of 0.8 A g^{-1} for 1000 cycles (Fig. 6d). Equivalent series resistance (ESR) is obtained by dividing the iR drop with the applied current density. ESR calculated for 1000 cycles are shown in Fig. 6d, and it is seen that the ESR in rGOSP20 is maintained almost constant and in the case of PANI, the value of ESR increases with cycles. The increase in ESR in PANI is expected due to the degradation of polymer backbone during repetitive charge–discharge cycling. Moreover, ESR value of rGOSP20 is found to be less compared to that of PANI. Hence, cycling stability for rGOSP20 is extended to 6000 cycles and the retention of capacity is found to be (75.2 %) with columbic efficiency of 98–100 %.

EIS is a very powerful tool for understanding the electrochemical behaviors of supercapacitors. Nyquist diagrams (Fig. 7) of the rGOSP composites show two distinct regions, the high-frequency distorted semicircle region, which transforms to a near-vertical spike in the low-frequency region. The high-frequency intercept on the real axis gives the ohmic resistance (R_s) of the materials; the diameter of the semicircle provides the charge transfer resistance (R_{ct}). The R_s values of the rGOSP composites are nearly the same (0.5 to 0.8 Ω). The R_{ct} value for rGOSP20, rGOSP40, rGOSP60, rGOSP80, and rGOSP100 is found to be 6.1, 6.6, 6.9, 7.8, and 8.7 Ω, respectively, and the R_{ct} value increases for the rGOSP composites as the rGOS content increases, which can be clearly seen in the inset of Fig. 7. The time constant for all the rGOSP composites is calculated from the maximum of the semicircle and found to be in the range of 0.6 to 0.9 ms. Low time constants (of the order of ms) are preferred for electrochemical supercapacitors in order to ensure fast charge–

Fig. 4 FESEM pictures of **a** rGO, **b** rGOS, and **c** rGOSP20; **d**, **e** TEM pictures of rGOSP20
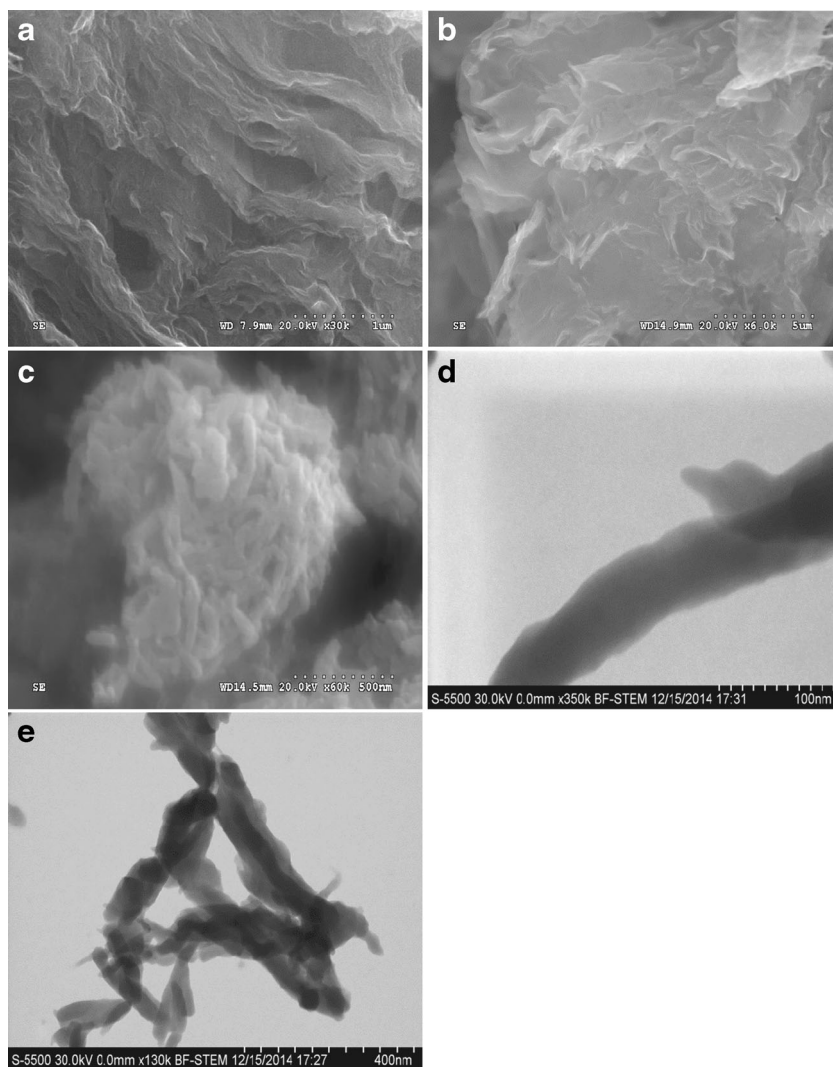
discharge characteristics [25, 26]. The straight line (near-vertical) in the low-frequency region reveals ion diffusion behavior of the electrolyte to the electrode surface. The very steep shape indicates the swift ion diffusion in solution and the adsorption onto the electrode surface [27].
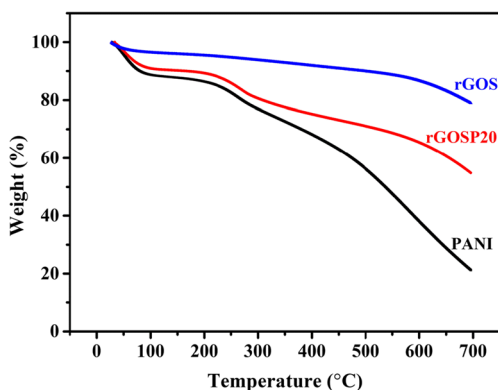

Fig. 5 Thermograms of PANI, rGOS, and rGOSP20

The equivalent circuit, showed as an inset in Fig. 7, is obtained from the simulation of the experimental data using ZMAN software supplied with the electrochemical worksta-tion. The circuit consists of R_s, R_{ct}, CPE_1, CPE_2 elements which are bulk solution resistance, charge transfer resistance, and constant phase elements, respectively. A similar equiva-lent circuit was also proposed for other PANI-based systems [28–31]. CPE_1 is related to the double-layer capacitance at the electrode surface, while CPE_2 corresponds to the pseudocapacitance of the electrode. The values of these pa-rameters are given in Table 2. The constant phase element (CPE) is defined as below

$$CPE = |Q(j\omega)^n|^{-1}$$

The constant Q is a combination of properties related to the surface and the electroactive species, while the exponent n arises from the slope of the log Z versus log f plot. The expo-nent n denotes the correction factor pertaining to the
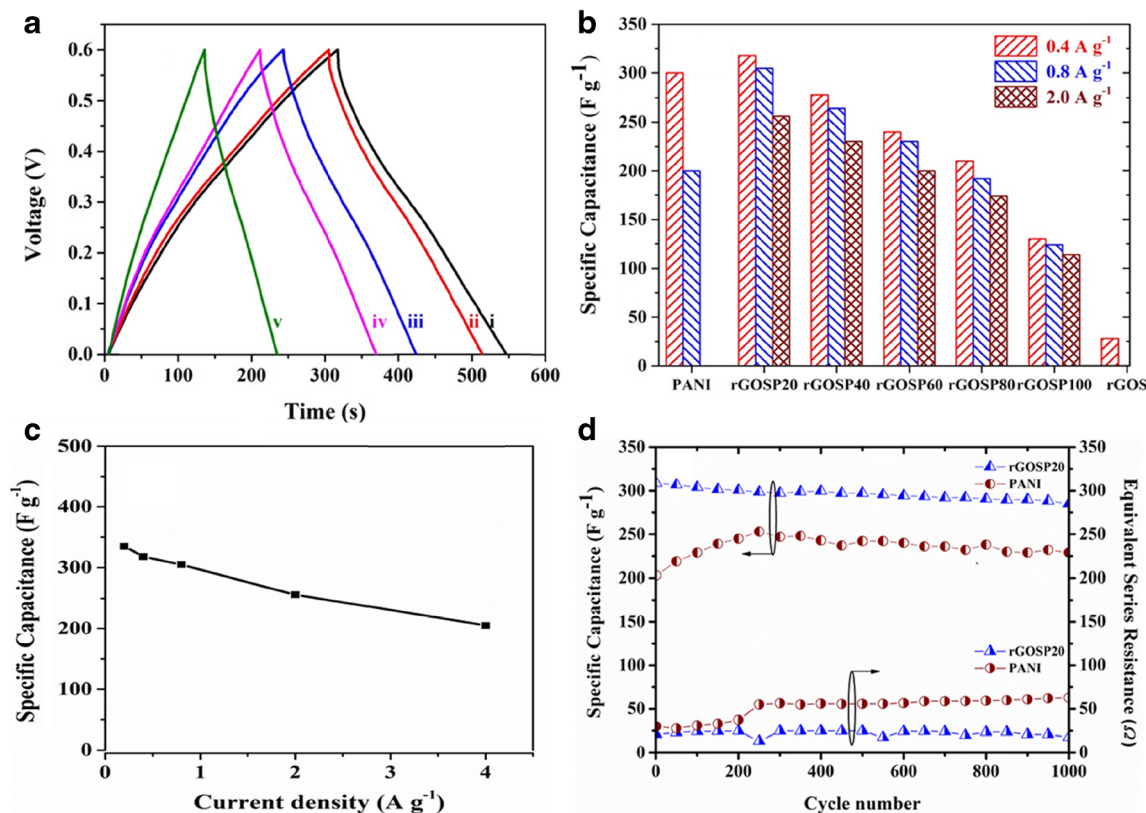
Fig. 6 a Galvanostatic charge–discharge curves of the rGOSP composites (*i*) rGOSP20, (*ii*) rGOSP40, (*iii*) rGOSP60, (*iv*) rGOSP80, and (*v*) rGOSP100 measured at an applied current density of 0.4 A g^{-1} in 1 M H$_2$SO$_4$ solution. **b** Comparison of the specific capacitance of rGOSP composites with rGOS and PANI measured at various applied current densities. **c** Behavior of specific capacitance with current density for rGOSP20. **d** Comparison of specific capacitance and ESR of symmetric rGOSP20 with PANI supercapacitor cells measured at an applied current density of 0.8 A g^{-1} in 1 M H$_2$SO$_4$ solution

roughness of the electrode and has values that range from −1 to 1. When $n = -1$ it represents pure inductive behavior, $n = 1$ it represents the pure capacitive behavior, when $n = 0$, it represents pure the resistor behavior, while $n = 0.5$ represents a Warburg impedance. In the present studies, n is greater than

0.9 for both the constant phase elements showing that the composite material behaves more like a capacitor.

Significantly higher capacitance with a good cycle life of rGOSP20 is due to the synergistic effect of all the materials present in the rGOSP composite wherein the intercalation of polyaniline into stable conductive rGOS composite, which helps in retarding the degradation of polymer chains during continuous charge–discharge cycling. Also, the presence of rGOS in the composite helps in the contact of electrode material with electrolyte and reduces *iR* drop, thereby resulting in an overall improvement of the supercapacitor cell.
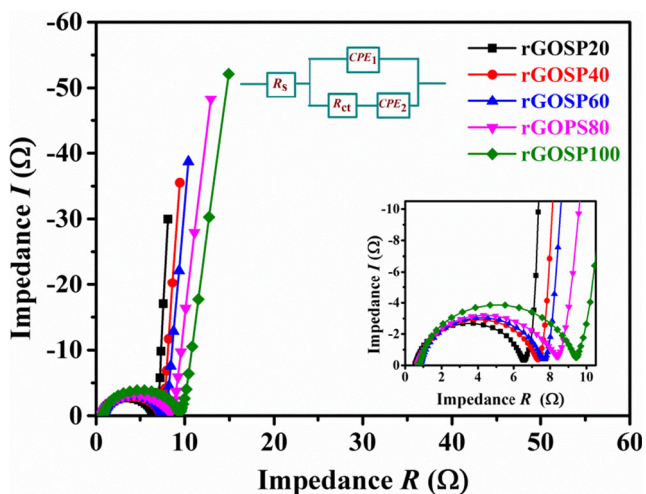
Fig. 7 Nyquist plots of different rGOSP composites (*insets* showing the expanded semicircle region and circuit diagram)

Table 2 Impedance parameters of reduced graphene oxide–silica–polyaniline composites

Sample	R_s (Ω)	R_{ct} (Ω)	CPE_1	n	CPE_2	n
rGOSP20	0.56	6.11	0.23	0.91	483	0.96
rGOSP40	0.78	6.62	0.23	0.92	404	0.96
rGOSP60	0.82	6.91	0.19	0.91	362	0.94
rGOSP80	0.65	7.86	0.35	0.86	278	0.94
rGOSP100	0.77	8.76	0.18	0.92	253	0.93

Conclusions

In this work, we have demonstrated the incorporation of graphene silica could help in improving the properties of polyaniline in terms of thermal stability, increasing its specific capacitance, reduction in ESR along with improved cycle life. This study is encouraging and might lead to further research of graphene silica-based ternary composites with different conducting polymeric systems for energy storage applications.

References

1. Brownson D, Banks C (2010) Graphene electrochemistry: an overview of potential applications. Analyst 135:2768–2778
2. Zhu Y, Murali S, Cai W, Li X, Suk J, Potts J, Ruoff R (2010) Graphene and graphene oxide: synthesis, properties, and applications. Adv Mater 22:3906–3924
3. Li C, Shi G (2011) Synthesis and electrochemical applications of the composites of conducting polymers and chemically converted graphene. Electrochim Acta 56:10737–10743
4. Kou L, Gao C (2011) Making silica nanoparticle-covered graphene oxide nanohybrids as general building blocks for large-area superhydrophilic coatings. Nanoscale 3:519–528
5. Salinas-Torres D, Montilla F, Huerta F, Morallon E (2011) All electrochemical synthesis of polyaniline/silica sol–gel materials. Electrochim Acta 56:3620–3625
6. Liu XX, Li YB, Bian LJ, Dou YQ, Huo YQ (2008) Electrodeposition of hybrid film of polyaniline/silica and its pseudocapacitive properties. J Solid State Electrochem 12:909–912
7. Zou H, Wu S, Shen J (2008) Polymer/silica nanocomposites: Preparation, characterization, properties, and applications. Chem Rev 108:3893–3957
8. Du X, Wang C, Li T, Chen M (2009) Studies on the performances of silica aerogel electrodes for the application of supercapacitor. Ionics 15:561–565
9. Feng X, Yan Z, Chen N, Zhang Y, Liu X, Ma Y, Yang X, Hou W (2013) Synthesis of a graphene/polyaniline/MCM-41 nanocomposite and its application as a supercapacitor. New J Chem 37:2203–2209
10. Chen GL, Shau SM, Juang TY, Lee RH, Chen CP, Suen SY, Jeng RJ (2011) Single-layered graphene oxide nanosheet/polyaniline hybrids fabricated through direct molecular exfoliation. Langmuir 27:14563–14569
11. Park S, An J, Potts J, Velamakanni A, Murali S, Ruoff R (2011) Hydrazine-reduction of graphite- and graphene oxide. Carbon 49:3019–3023
12. Sydulu S, Palaniappan S, Srinivas P (2013) Nano fibre polyaniline containing long chain and small molecule dopants and carbon composites for supercapacitor. Electrochim Acta 95:251–259
13. Zheng Z, Du Y, Feng Q, Wang Z, Wang C (2012) Facile method to prepare Pd/graphene–polyaniline nanocomposite and used as new electrode material for electrochemical sensing. J Mol Catal A: Chem 353:80–86
14. Ciric-Marjanovic G, Dragicevic L, Milojevic M, Mojovic M, Mentus S, Dojcinovic B, Marjanovic B, Stejskal J (2009) Synthesis and characterization of self-assembled polyaniline nanotubes/silica nanocomposites. J Phys Chem B 113:7116–7127
15. Yan J, Wei T, Shao B, Fan Z, Qian W, Zhang M, Wei F (2010) Preparation of a graphene nanosheet/polyaniline composite with high specific capacitance. Carbon 48:487–493
16. Huang Y, Lin C (2012) Polyaniline-intercalated graphene oxide sheet and its transition to a nanotube through a self-curling process. Polymer 53:1079–1085
17. Guardia L, Suárez-García F, Paredes JI, Solís-Fernández P, Rozada R, Fernández-Merino MJ, Martínez-Alonso A, Tascón JMD (2012) Synthesis and characterization of graphene–mesoporous silica nanoparticle hybrids. Microporous Mesoporous Mater 160:18–24
18. Kim KS, Park SJ (2011) Influence of multi-walled carbon nanotubes on the electrochemical performance of graphene nanocomposites for supercapacitor electrodes. Electrochim Acta 56:1629–1635
19. Zhou HH, Chen H, Luo SL, Lu GW, Wei WZ, Kuang YF (2005) The effect of the polyaniline morphology on the performance of polyaniline supercapacitors. J Solid State Electrochem 9:574–580
20. Uppugalla S, Male U, Srinivasan P (2014) Design and synthesis of heteroatoms doped carbon/polyaniline hybrid material for high performance electrode in supercapacitor application. Electrochim Acta 146:242–248
21. Male U, Singu BS, Srinivasan P (2015) Aqueous, interfacial, and electrochemical polymerization pathways of aniline with thiophene: Nano size materials for supercapacitor. J Appl Polym Sci 132:42013
22. Ragupathy P, Park DH, Campet G, Vasan HN, Hwang SJ, Choy JH, Munichandraiah N (2009) Remarkable capacity retention of nanostructured manganese oxide upon cycling as an electrode material for supercapacitor. J Phys Chem C 113:6303–6309
23. Wang YT, Lu AH, Zhang HL, Li WC (2011) Synthesis of nanostructured mesoporous manganese oxides with three-dimensional frameworks and their application in supercapacitors. J Phys Chem C 115:5413–5421
24. Hu C, Li W, Lin J (2004) The capacitive characteristics of supercapacitors consisting of activated carbon fabric–polyaniline composites in NaNO3. J Power Sources 137:152–157
25. Burke A (2000) Ultracapacitors: why, how, and where is the technology. J Power Sources 91:37–50
26. Singu B, Male U, Srinivasan P, Pabba S (2014) Use of surfactant in aniline polymerization with TiO2 to PANI-TiO2 for supercapacitor performance. J Solid State Electrochem 18:1995–2003
27. Ma RZ, Liang J, Wei BQ, Zhang B, Xu CL, Wu DH (1999) Study of electrochemical capacitors utilizing carbon nanotube electrodes. J Power Sources 84:126–129
28. Metikos-Hukovic M, Omanovic S (1998) Thin indium oxide film formation and growth: impedance spectroscopy and cyclic voltammetry investigations. J Electroanal Chem 455:181–189
29. Girija TC, Sangaranarayanan MV (2006) Analysis of polyaniline-based nickel electrodes for electrochemical supercapacitors. J Power Sources 156:705–711
30. Girija TC, Sangaranarayanan MV (2006) Polyaniline-based nickel electrodes for electrochemical supercapacitors—influence of Triton X-100. J Power Sources 159:1519–1526
31. Guan H, Fan LZ, Zhang HC, Qu XH (2010) Polyaniline nanofibers obtained by interfacial polymerization for high-rate supercapacitors. Electrochim Acta 56:964–968